Microscopic structure of the hydrogen-xenon mixture

R. Senesi, M. Nardone, F. P. Ricci, and M. A. Ricci
Dipartimento di Fisica ''Edoardo Amaldi,'' Università degli Studi di Roma Tre, Unità dell' Istituto Nazionale per la Fisica della Materia, via della Vasca Navale 84, 00146 Roma, Italy

A. K. Soper*
ISIS Facility, Rutherford Appleton Laboratory, Chilton, Didcot, Oxfordshire OX11 0QX, United Kingdom
(Received 12 March 1997)

We report a neutron-diffraction study of the microscopic structure of the H_2-Xe binary mixture in the Xe-rich phase, $x_{Xe}=0.78$, at $T=283$ K and $P=170$ bars, i.e., in the vicinity of the second-type gas-gas demixing surface. The site-site distribution functions are extracted employing the H-D isotopic substitution technique. We report also molecular-dynamics simulations for a mixture of equivalent Lennard-Jones (LJ) atoms. The experimental results are compared with previous ones obtained for the He-Xe and Ne-Xe mixtures, which show a first- and a second-type gas-gas transition, respectively. The general picture already suggested by the other two mixtures agrees also with the present results, although in this case the center-center distribution functions H_2-H_2 and H_2-Xe are clearly modulated by the Xe-Xe correlations. In particular the features found in the distribution functions of the mixture suggest that the LJ potential model is not able to reproduce at a satisfactory level the H_2-H_2 and the H_2-Xe correlation functions and that a (XeH_4) chemical complex is present. [S1063-651X(97)08309-8]

PACS number(s): 61.20.Ja, 61.12.−q, 61.20.Ne

I. INTRODUCTION

Supercritical fluids and fluid mixtures are relevant to both applied and basic science. In particular, gas-gas demixing phase transitions may occur in binary mixtures of simple fluids provided that the interaction potential parameters of the two components are strongly different. Such transitions are inherent in the van der Waals equation of state and, although already foreseen at the beginning of the century, they were observed for the first time only in the 1950s [1].

Different behaviors of the critical line of the demixing phase transitions have been found also in mixtures of simple fluids. These behaviors are referred to in the literature [1] as first-type and second-type gas-gas phase transitions, according to the initial slope of the P-T projection of the critical line. In particular, for the transition of the first type $(\partial P/\partial T)_c$ (where the subscript c indicates that the derivatives are taken along the critical line) is positive, as in the case of the He-Xe mixture [2], whereas it is negative for the second-type ones such as those found in Ne-Xe [3] and H_2-Xe mixtures [4]. First- and second-type demixing transitions differ also for the sign of $(\partial T/\partial x)_c$, where x is the molar fraction of the less volatile component (i.e., Xe in the above-quoted examples). Indeed, since for gas-gas demixing transitions $(\partial P/\partial x)_c$ is always negative, in a second-type transition the critical temperature increases with x, while the contrary happens for a first-type transition.

It is reasonable to assume that difference in the sign of $(\partial P/\partial T)_c$ will be related to differences in the microscopic structure of the mixtures, described by the site-site distribution functions (i.e., $g_{\alpha\alpha}$, $g_{\beta\beta}$, and $g_{\alpha\beta}$ for a binary α-β mixture). These can be measured by a neutron-diffraction experiment, if the isotopic substitution technique is possible, or evaluated by molecular-dynamics (MD) simulation, if intermolecular potentials good enough to reproduce the experimental total neutron weighted radial distribution function are available. Until now only two diffraction experiments aimed at studying the influence of the microscopic structure on the gas-gas phase transition have been published. These were performed respectively on He-Xe [5] and Ne-Xe [6] mixtures, at the same corresponding thermodynamic state. Since in these cases the isotopic substitution technique was not feasible, the site-site distribution functions were extracted by combining neutron-diffraction and MD simulation experiments.

In this paper we address the issue of determining the microscopic structure of another mixture that exhibits a second-type gas-gas demixing transition, namely, the H_2-Xe one. In this case we can take full advantage of the isotopic hydrogen-deuterium substitution in the neutron-diffraction experiment and obtain the experimental site-site distribution functions, without resorting to MD simulation.

II. EXPERIMENT AND DATA ANALYSIS

Several isobaric sections of the demixing surface of the H_2-Xe mixture have been determined, measuring the refractive index of the coexisting phases [4]. From the curves reported in Fig. 1 we find $(\partial P/\partial T)_c \simeq -12$ bars/K; this value must be compared with -16 and $+35$ bar/K, which are the analogous quantities found for the Ne-Xe and He-Xe mixtures, respectively. The thermodynamical state chosen for the present neutron-diffraction experiment is at $T=283$ K, $P=170$ bars, and $x_{Xe}=0.78$ and its position relative to the demixing transition is shown in Fig. 1. These thermodynamic state parameters have been chosen following the cor-

*Also at Department of Physics and Astronomy, University College London, Gower Street, London WC1E 6BT, United Kingdom.

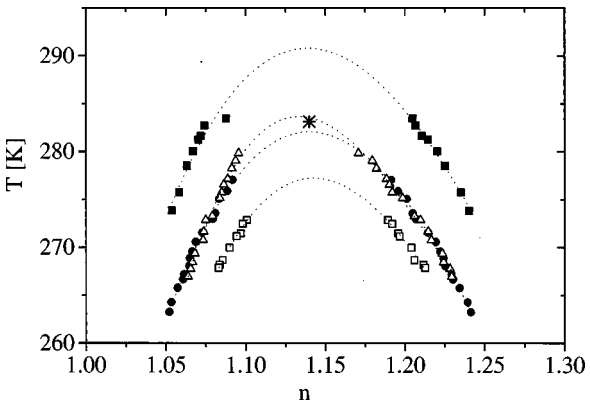

FIG. 1. Behavior of the refractive index n of the two coexisting phases of the H_2-Xe mixture at four isobaric sections of the demixing surface: $p=72$ bars (full squares), $p=154$ bars (open triangles), $p=170$ bars (full circles), and $p=215$ bars (open squares). The dotted curve represents the best fit to the experimental data using $n_1-n_2=A(T-T_c)^{\beta}$. The value of β is fixed at 0.33, while A and T_c are fitted to each curve. The asterisk refers to the thermodynamic state at which we performed our neutron-scattering experiment ($P=170$ bars).

responding state principle in order to map, in the present case, a thermodynamic state that is nearly the same as the one already studied for both the He-Xe and the Ne-Xe mixtures [5,6].

Gas samples, of 99.995% purity, were supplied by the Matheson Co. The mixtures were prepared, as previously done [5,6], in a reservoir (having a volume V_r) using the following procedure.

(i) The empty reservoir is kept at a fixed temperature ($T=298$ K) and filled with an appropriate quantity of pure Xe, the density of which (ρ_{gas}^{Xe}) is determined from available thermodynamic data [7].

(ii) The reservoir is then cooled down to 77 K so that the Xe content solidifies, occupying a volume $V=V_r(\rho_{gas}^{\mathrm{Xe}}/\rho_{solid}^{\mathrm{Xe}})$, where $\rho_{solid}^{\mathrm{Xe}}$ is the density of solid Xe at $T=77$ K [8].

(iii) The empty volume of the reservoir (V_r-V) is then filled at 77 K with H_2 until its pressure reaches the value required [9] in order to have $\rho_{\mathrm{H_2}}=(1/x_{\mathrm{Xe}}-1)/(1/\rho_{gas}^{\mathrm{Xe}}-1/\rho_{solid}^{\mathrm{Xe}})$, which then yields the desired mixture.

(iv) The reservoir is finally heated above the demixing temperature. The homogeneity of the mixture is favored, stimulating convective motion, by the application of thermal gradients opposite to the gravitational field.

Several days before the neutron-diffraction experiment three different reservoirs were prepared, one for each sample, i.e., D_2-Xe, H_2-Xe, and H_2-D_2-Xe. The concentration of Xe in all the mixtures was $x_{\mathrm{Xe}}=0.78$ and in the case of the H_2-D_2-Xe mixture both $x_{\mathrm{H_2}}$ and $x_{\mathrm{D_2}}$ were equal to 0.11.

The neutron-diffraction experiment was performed on the SANDALS diffractometer, installed at the ISIS pulsed neutron source (Rutherford Appleton Laboratory). This is a small angle ($3°\leqslant 2\theta \leqslant 21°$) time-of-flight diffractometer suited for studies of liquid and amorphous samples. Its setup and the advantages of using neutrons from a spallation source have already been published elsewhere [10].

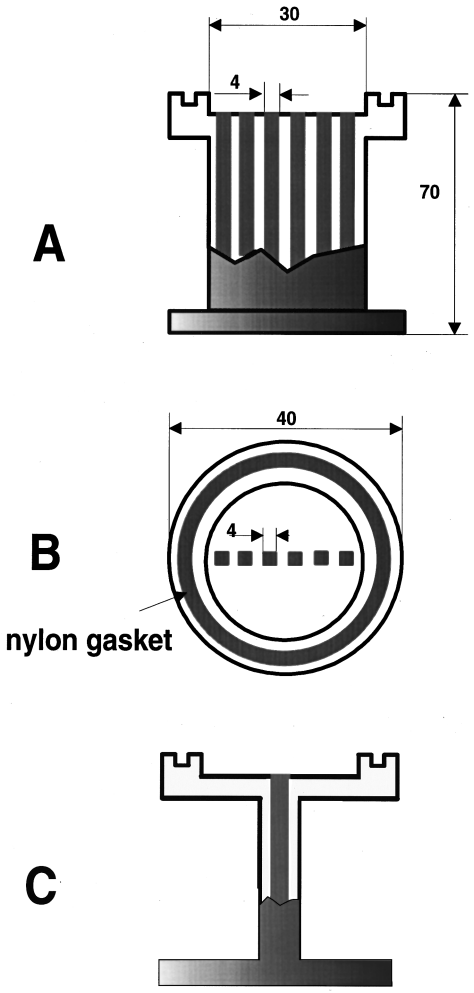

FIG. 2. Front (A), top (B), and side (C) views of the sample container. The dimensions are quoted in millimeters. The container is clamped to two flanges. The one on the top contains the gas inlet tube.

The sample container was machined from a Ti-Zr ''null'' alloy rod (see Fig. 2). In the slab (6 mm thickness) shaped central part an array of six square (4×4 mm^2) holes contains the scattering sample. The container design is a good compromise between the need of having enough sample in the beam area and safely withstanding a pressure of 200 bars. The sample container was in thermal contact with a copper frame, the temperature of which was regulated by circulation of a liquid refrigerant. Two platinum resistors, placed between the copper frame and the sample container at the top and bottom flanges, respectively, were used in order to measure the sample temperature: this was stable at 283.0 ± 0.1 K during the experiment. The sample pressure, measured by a strain gauge, was 170 ± 1 bars and corresponds to a Xe partial density of 0.83×10^{-2} mole/cm^3 [4].

The measurements on each mixture lasted roughly 24 h, during which several runs were recorded in order to check that the data reproducibility was well within the statistical uncertainty. Measurements on the empty sample container (12 h) as well as on a standard vanadium slab and background were also performed.

The raw data have been corrected for multiple scattering, absorption, background and sample container contributions,

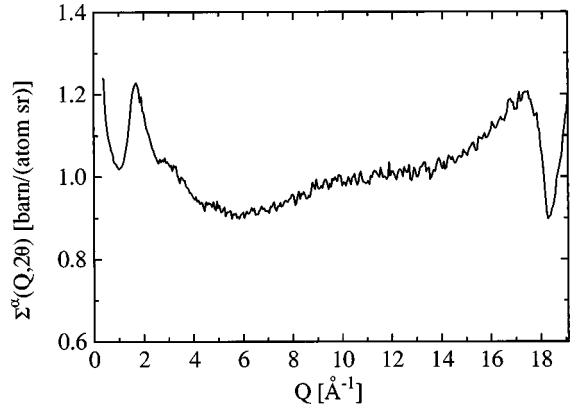

FIG. 3. Measured differential cross-section of the D_2-Xe sample at $2\vartheta = 20°$ as a function of the magnitude of the elastically exchanged wave vector.

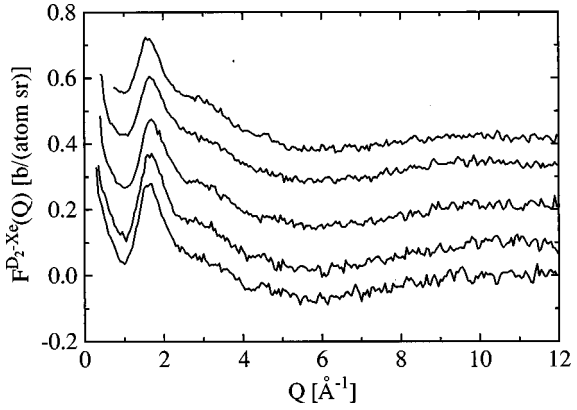

FIG. 4. The interference scattering cross section for the D_2-Xe sample at the different 2ϑ values. The scattering angle decreases going from the bottom to the top (the curves are shifted by 0.1 b/sr atom).

following the standard procedure outlined in Ref. [11]. This leads to the determination, for each mixture α, of the differential cross section $\Sigma^{\alpha}(Q,2\theta)$, where Q is the magnitude of the wave-vector transfer and 2θ the scattering angle. An example of $\Sigma^{\alpha}(Q,2\theta)$ is reported in Fig. 3. Bearing in mind the presence of inelastic contributions in the atomic self-scattering and the presence of resonances in the neutron scattering from Xe in the region 8–16 eV, we can write

$$\Sigma^{\alpha}(Q,2\theta) = F^{\alpha}(Q) + \Sigma^{\alpha}_{self}(Q,2\theta) + \Sigma^{\alpha}_{res}(Q,2\theta), \quad (1)$$

where $F^{\alpha}(Q)$ is the interference scattering cross section, which does not depend on the diffraction angle 2θ (i.e., on the detector bank), $\Sigma^{\alpha}_{self}(Q,2\theta)$ represents the atomic self-scattering contribution and $\Sigma^{\alpha}_{res}(Q,2\theta)$ the contribution to the scattering due to the Xe absorption. The two latter contributions are angle dependent since they are determined by the energy exchange. The presence of the so-called inelasticity effects, in $\Sigma^{\alpha}_{self}(Q,2\theta)$, are relevant in the case of light atoms and strongly determined by the experimental geometry [12]. In this respect the availability of neutron detectors at low angles, as in the case of SANDALS, is indeed of great help when dealing with hydrogen-containing samples since in these conditions the systematic error due to the inelastic effects is strongly reduced. Unfortunately, in the present experiment we could not use the lowest detector banks, owing to the presence of $\Sigma^{\alpha}_{res}(Q,2\theta)$. Its signature, which appears at $Q \geqslant 16$ Å at $2\vartheta = 20°$ (see Fig. 3), shifts towards lower- Q values as 2ϑ decreases. As a consequence, only five detector banks, out of the ten available on SANDALS at the time of the experiment, were useful and the available Q range was *de facto* shortened down to 12 Å^{-1}. As a consequence, of these limitations, it should be emphasized that the quality and statistical accuracy of the final results are below the present performance of SANDALS.

In order to extract the interference scattering cross section $F^{\alpha}(Q)$, we proceeded as follows.

(i) For each sample at each detector bank (i.e., 2θ values) the measured differential cross section, expressed as a function of the incident neutron energy E, was fitted with the expression

$$\Sigma^{\alpha}(Q,2\theta) = a^{\alpha}(2\theta) + b^{\alpha}(2\theta)\frac{(E_0 - E)}{(E_0 - E)^2 + \Gamma^2} \quad (2)$$

in the region where the interference contribution $F^{\alpha}(Q)$ is negligible (i.e., 4.2 eV$\leqslant E \leqslant$8.7 eV). In Eq. (2) $a^{\alpha}(2\theta)$ accounts for the high-Q level of the atomic self-scattering, E_0 and Γ are the energy and width of the resonance, respectively, and $b^{\alpha}(2\theta)$ is a normalization factor. As far as the values of the best-fit parameters are concerned, E_0 is found to agree within a few percent with the value quoted in the literature [13,14], while Γ appears to be underestimated by some 30%. This rather poor agreement in $\Gamma$is not surprising since we are fitting only the low-energy tail of the resonance.

(ii) From the measured differential cross section we subtract the extrapolation of $\Sigma^{\alpha}(Q,2\theta)$ in the 0 eV$\leqslant E \leqslant$8.7 eV range. Then we correct for inelasticity effects, fitting what remains, at each 2θ value, with a stretched exponential basically following the procedure already described [15]. The final result is $F^{\alpha}(Q)$.

The reliability of the procedure followed is checked (see Fig. 4) by looking at the reproducibility of the $F^{\alpha}(Q)$'s obtained at the different 2θ values: as a matter of fact both inelastic contributions and resonances effects appear at 2θ-dependent Q values, in contrast with the genuine features of the interference scattering. The $F^{\alpha}(Q)$'s obtained at the different detector banks were merged together and are shown in Fig. 5 for the three samples. These can be expressed as linear combinations of the partial structure factors (PSF's) $H_{ij}(Q)$ given by

$$H_{ij}(Q) = \delta_{ij} + \sqrt{\rho_i \rho_j}\int [g_{ij}(r) - 1]\exp(-i\vec{Q}\cdot\vec{r})d\vec{r}, \quad (3)$$

where $g_{ij}(r)$ are the intermolecular site-site distribution functions (ISSDF's); ρ_i and ρ_j are the atomic number densities of species i and j. The $F^{\alpha}(Q)$'s may then be written as

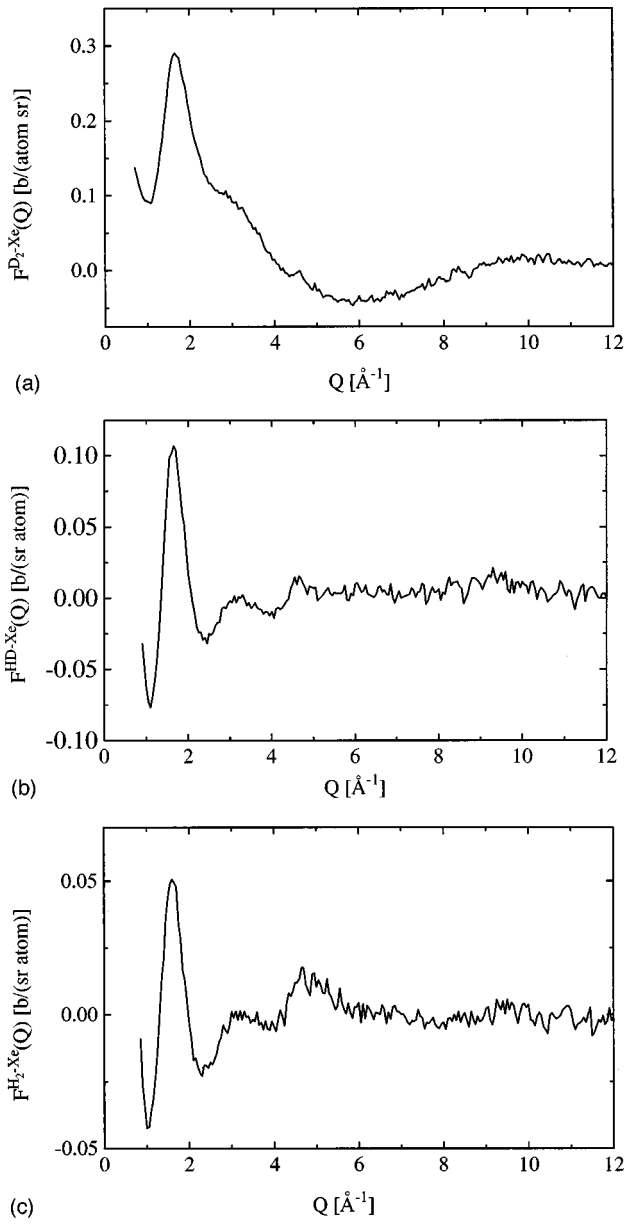

FIG. 5. Interference scattering cross section obtained after merging the data collected at six different diffraction angles, for three samples: (a) the D_2-Xe mixture; (b) the equimolar mixture of the two, labeled HD-Xe; and (c) the H_2-Xe mixture.

$$F^{D_2\text{-Xe}}(Q)=x_{Xe}b_{Xe}^2H_{Xe\text{-}Xe}(Q)+2x_{D_2}b_D^2H_{H\text{-}H}(Q)+2\sqrt{2x_{Xe}x_{D_2}}b_{Xe}b_DH_{Xe\text{-}H}(Q)+2x_{D_2}b_D^2\frac{\sin(Qd)}{Qd}, \quad (4)$$

$$F^{H_2\text{-Xe}}(Q)=x_{Xe}b_{Xe}^2H_{Xe\text{-}Xe}(Q)+2x_{H_2}b_H^2H_{H\text{-}H}(Q)+2\sqrt{2x_{Xe}x_{H_2}}b_{Xe}b_HH_{Xe\text{-}H}(Q)+2x_{H_2}b_H^2\frac{\sin(Qd)}{Qd}, \quad (5)$$

$$F^{HD\text{-Xe}}(Q)=x_{Xe}b_{Xe}^2H_{Xe\text{-}Xe}(Q)+2x_{H_2}\overline{b^2}H_{H\text{-}H}(Q)+2\sqrt{2x_{Xe}x_{H_2}}b_{Xe}\overline{b}H_{Xe\text{-}H}(Q)+2x_{H_2}(2k^{1/2}+1)^{-1}[(b_H^2+b_D^2)k^{1/2}+b_Hb_D]\frac{\sin(Qd)}{Qd}, \quad (6)$$

where $x_{H_2}=x_{D_2}=0.22$, b_{Xe}, b_D, and b_H are the atomic scattering lengths for the three atomic species [13], and $\overline{b}$ is equal to $(b_H+b_D)/2$; d is the intramolecular H-H distance and k is the value of the equilibrium constant for the H-D exchange reaction. Due to the high value of the dissociation energy of the hydrogen molecules, no exchange reaction should in principle occur at room temperature ($k=\infty$); nevertheless, the metallic reservoir itself may behave as a catalyst for the H-D exchange. As a matter of fact, our experimental data for $F^{HD\text{-Xe}}(Q)$, fitted in the high-Q region where the value of the $H_{ij}(Q)$ functions is negligible, are compatible with a random distribution of the two isotopes ($k=1/4$).

From Eqs. (4)–(6) we have extracted the PSF's and evaluated the radial pair distribution functions. The conversion to r space has been performed using a minimum noise algorithm, instead of a direct Fourier transform, since this method is particularly suited when noisy data have to be treated [16].

The ISSDF's are obtained after subtraction of the intramolecular peak, which is very sharp and well separated from the intermolecular contribution. We note that the H-H intramolecular distance obtained from our data turns out to be $d=0.74$ Å, in agreement with the value quoted in the literature [17].

We have also performed MD simulations of a mixture of Lennard-Jones (LJ) atoms equivalent to our sample. In these simulations we followed the dynamics of a mixture of 390 Xe particles and 110 particles equivalent to the centers, c, of the hydrogen molecule over a time interval of 250 ps, after having equilibrated at the same thermodynamic state as the experimental one for 250 ps. The time step was 50 fs. In the MD first simulation, hereafter referred to as MDI, the LJ potential parameters used were $\sigma_{C\text{-}C}=2.72$ Å, $\sigma_{Xe\text{-}Xe}=3.85$ Å, $(\epsilon/k_B)_{C\text{-}C}=36.2$ K, $(\epsilon/k_B)_{Xe\text{-}Xe}=237$ K. In a second MD simulation, hereafter referred to as MDII, we used the same potential parameters except for σ_{CC}, which was chosen to be 3.3 Å. In both cases the parameters of the unlike pairs were calculated following the Lorentz-Berthelot rule, as done by Bellissent-Funel *et al.* [5]. Although the σ_{CC} value more frequently reported in the literature [18] is $\sigma_{C\text{-}C}=2.72$ Å, we performed MDII following the indications of our experimental $g_{C\text{-}C}(r)$, as will be discussed later. It is important to note that $g_{Xe\text{-}Xe}(r)$ is practically the same in both simulations, as should have been expected. As far as $g_{C\text{-}Xe}(r)$ and $g_{C\text{-}C}(r)$ are concerned, going from MDI to MDII, the only change is a shift on the r axis, while the overall shape remains the same as shown in Figs. 6(b) and 6(c).

III. DISCUSSION

The comparison of our data with the present MD simulations and with the results reported for the He-Xe and Ne-Xe

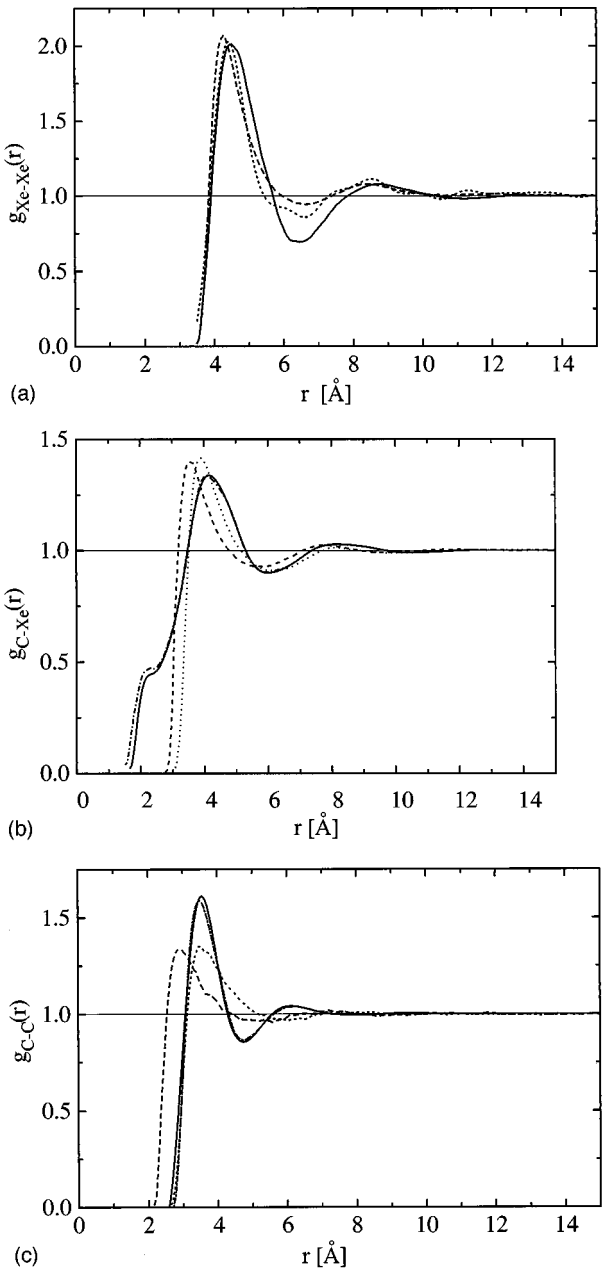

FIG. 6. (a) Site-site distribution function for the Xe atoms from the present experiment (full line) compared with the results of the MD simulation (dashed line) and with that reported in Ref. [5] for pure Xe (dotted line) at the same Xe number density. (b) $g_{C\text{-}Xe}(r)$ function (full line), as obtained from the experimental $g_{H\text{-}Xe}(r)$ (dash-dotted line), compared with the results of the MDI (dashed line) and MDII (dotted line) simulations. (c) $g_{C\text{-}C}(r)$ function (full line), as obtained from the experimental $g_{H\text{-}H}(r)$ (dash-dotted line), compared with the results of the MDI (dashed line) and MDII (dotted line) simulations.

mixtures [5,6] is more properly performed by looking at the radial distribution functions of the centers of mass of the two components, namely, $g_{Xe\text{-}Xe}(r)$, and the two functions involving the center of mass C of the hydrogen molecule, $g_{C\text{-}C}(r)$ and $g_{C\text{-}Xe}(r)$, respectively. These functions can be extracted from the ISSDF's $g_{H\text{-}H}(r)$ and $g_{H\text{-}Xe}(r)$, assuming that orientational correlations between H_2 molecules are absent. The above assumption is reasonable since the anisotropy of both the hard-core and long-range intermolecular potential is very low. Under this assumption the functions $g_{Xe\text{-}C}(r)$ and $g_{C\text{-}C}(r)$ are given by [19]

$$g_{Xe\text{-}C}(r)-1=\frac{1}{(2\pi)^2\sqrt{\rho_{Xe}\rho_H}}\int\frac{H_{Xe\text{-}H}(Q)}{\frac{\sin(Qd/2)}{Qd/2}}\exp(-i\vec{Q}\cdot\vec{r})d\vec{Q} \tag{7}$$

$$g_{C\text{-}C}(r)-1=\frac{1}{(2\pi)^2\rho_H}\int\frac{H_{H\text{-}H}(Q)}{\left(\frac{\sin(Qd/2)}{Qd/2}\right)^2}\times\exp(-i\vec{Q}\cdot\vec{r})d\vec{Q}. \tag{8}$$

As shown in Figs. 6(b) and 6(c), these two radial distribution functions differ only slightly from $g_{H\text{-}Xe}(r)$ and $g_{H\text{-}H}(r)$, respectively, since the intramolecular distance d is quite small.

As a first step we compare our experimental $g_{Xe\text{-}Xe}(r)$, $g_{Xe\text{-}C}(r)$, and $g_{C\text{-}C}(r)$ with the MD results. In Fig. 6(a) we report the experimental and simulated $g_{Xe\text{-}Xe}(r)$ in the mixture together with the one of pure Xe at almost the same Xe number density. As we can see from Fig. 6(a), there is overall agreement between the three functions, although minor differences are detectable between our data and the MD results: in the experimental data the first peak of $g_{Xe\text{-}Xe}(r)$ is indeed slightly broader and the first minimum is clearly more pronounced.

Much more impressive is the disagreement, shown in Fig. 6(c), between experimental and simulated $g_{C\text{-}C}(r)$. In particular, MDI shows the minimum approach distance and the first peak position at a definitely lower-r value and presents an asymmetric long-distance tail, as expected for a low-density gas, while the shape of the experimental $g_{C\text{-}C}(r)$ function is more liquidlike. It is worth noting that by using MDII parameters only the minimum approach distance and peak position can be recovered, but the overall disagreement between experiment and simulation remains.

Similar significant differences between experiment and simulation are present also in the $g_{Xe\text{-}C}(r)$ function [see Fig. 6(b)]. Moreover another discrepancy is evident in the region around 2.3 Å. The physical interpretation of this extra intensity found experimentally at distances shorter than 3 Å is far from being obvious. If we assume that systematic errors are not the origin of this feature, then it is likely to be due to the presence of a chemical complex involving hydrogen atoms around a xenon one ($Xe\text{-}H_n$). If this is the case, the shoulder must be analyzed as a separate peak, located at roughly 2.3 Å with an area corresponding to ~ 0.07 hydrogen atoms around a central Xe atom. This would imply that if we assume, for instance, $n=4$, about 1.5% of the Xe atoms are involved in such molecular aggregates.

Finally, a comparison between the experimental neutron weighted $g(r)$ with the analogous function obtained by MD simulations is shown in Fig. 7. As might have been anticipated, the neutron weighted $g(r)$ is not satisfactorily reproduced by either MD simulation. We recall that this lack of agreement between experiment and MD simulation was not present in either He-Xe or Ne-Xe mixtures [5,6]. For this

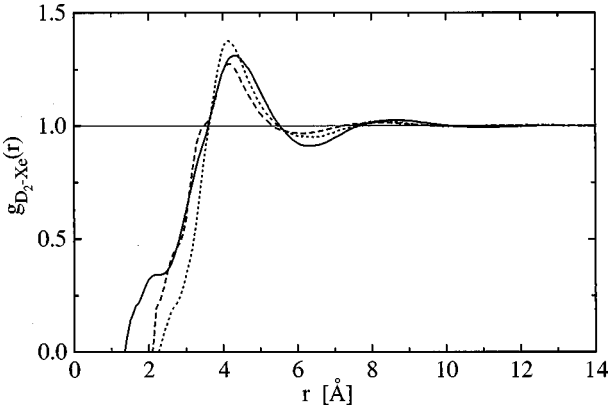

FIG. 7. Experimental total ''neutron weighted'' $g(r)$ for the D_2-Xe mixture (full line) compared with that calculated from MDI (dashed line) and MDII (dotted line) simulations.

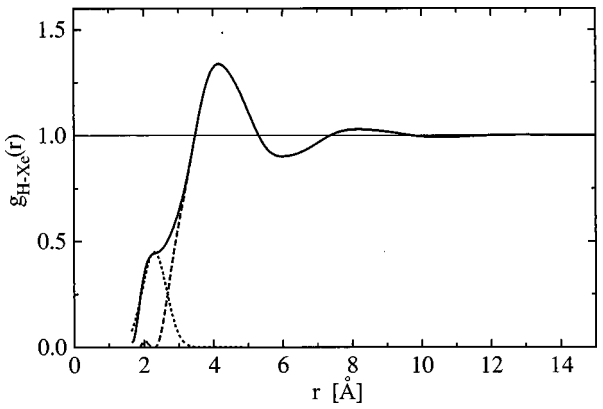

FIG. 8. $g_{\text{H-Xe}}(r)$ function (full line) decomposed in intramolecular correlations, assigned to XeH_n complex (dotted line), and in intermolecular ones $g^0_{C\text{-}Xe}(r)$ (dashed line).

reason we were confident that in those cases the ISSDF's calculated by MD simulation, which used a potential model, were reliable. On the contrary, in the present case we must conclude that, at least in the thermodynamic state studied here, the LJ potential model is not a good representation of the intermolecular interactions in the H_2-Xe mixture essentially as far as H_2-H_2 and H_2-Xe interactions are concerned.

It is worth emphasizing that the structural discrepancy between experiment and simulation is seen in both the *C*-*C* and Xe-*C* radial distribution functions. Systematic errors are believed to be at a minimum for the H-H (= *C*-*C*) distribution because the residual uncertainties from the inelasticity effects cancel to a very good approximation for this distribution. This important result implies that until a more accurate interatomic potential is developed, any consideration of the microscopic structure of the H_2-Xe mixture is reliable only if we use the experimental ISSDF's. We will therefore rely on the features of our experimental $g_{ij}(r)$ in order to derive information on the microscopic structure of the H_2-Xe mixture and its relationship to the behavior of the critical demixing surface.

IV. Xe-Xe CORRELATIONS

As we can see from Fig. 6(a), the Xe-Xe correlations in the mixture, mainly as far as the overall shape is concerned, appear to be weekly affected by the presence of the H_2 molecules. In fact, the Xe-Xe correlations, in the mixture are very similar to those measured in pure Xe at the same Xe number density [5]. Since this behavior has also been found in the He-Xe and Ne-Xe mixtures [5,6] we conclude that, at least when the Xe concentration is $\sim$80%, the structure of the Xe network is the same in all the three supercritical mixtures. We note that in all three cases an equal value of $\sim$5.6 Xe atoms is found for the nearest neighbors around a Xe atom.

V. H_2-H_2 CORRELATIONS

These correlations are given by the experimental $g_{cc}(r)$. As we can see from Fig. 6(c), the experimental function shows clear oscillations beyond the first maximum. In both computer simulations the position of this peak is determined mainly by the two-body *C*-*C* effective intermolecular interaction, that is, it is consistent with the respective values of $\sigma_{C\text{-}C}$. Beyond this peak the structure damps away in the manner of a simple liquid. For the experiment we note that the successive oscillations are similar in period to the Xe-Xe correlations, although they appear to be in opposite phase to them. Therefore, considering also Fig. 6(b), the H_2 molecules show a tendency to be located in shells where minima for the Xe atom distribution occur. These characteristics are peculiar of the H_2-Xe mixture and may be a consequence of the much larger effective hard-core dimension of H_2 molecules with respect to those of He and Ne.

VI. H_2-Xe CORRELATIONS

As already pointed out in discussing the comparison of our experimental results with MD simulations, the $g_{\text{H-Xe}}(r)$ distribution function reported in Fig. 6(b) can be considered to arise essentially from two distinct contributions, one corresponding to the Xe-H_n molecular complex, the other related to intermolecular H_2-Xe correlations $g^0_{\text{H-Xe}}(r)$. The latter is obtained from $g_{\text{H-Xe}}(r)$ after subtraction of the contribution due to the molecular Xe-H_n complex, fitted with a Gaussian distribution. This subtraction can be done quite safely since the intramolecular correlations are relevant in an r range where the intermolecular ones are negligible. In Fig. 8 we report the result of such a decomposition. Furthermore, as already discussed for the H-H correlations [see Fig. 6(b)], we feel safe to interpret the intermolecular contribution in terms of correlations between the molecular center of mass *C* and the Xe atom, namely, $g^0_{\text{C-Xe}}(r)$.

We note that, as in the case of H_2-H_2 correlations, $g^0_{\text{C-Xe}}(r)$ beyond the first peak shows oscillations that are clearly determined by the Xe-Xe correlations. Again these oscillations are peculiar of the H_2-Xe mixture, while they were absent in both He-Xe and Ne-Xe mixtures. However, we want to stress that, as in the cases of the He-Xe and Ne-Xe mixtures, there is a clear overlap between the Xe-H_2 and Xe-Xe first neighbor shells (assuming a Xe atom to be located at the origin). Following the procedure of Ref. [6], we calculated the fraction f of H_2 molecule first neighbors that do not overlap the first-neighbor Xe shell (i.e., the H_2 molecules located at $r \leqslant 3.5$ Å) to be $f = 0.14$. It is interesting

to compare this value with the much larger values found for He-Xe and Ne-Xe mixtures, which were 0.63 and 0.45, respectively [5,6].

VII. CONCLUSION

Here we summarize the most relevant results of the present experiment and further clarify the connections between the features of the microscopic structure and the peculiarities of the demixing phase transition in supercritical mixtures. We start by considering the two unexpected results that are peculiar of the H_2-Xe mixture.

The first result is the evidence of molecular complexes of the type Xe-H_n, although in quite low concentration, as shown in Fig. 6(b). Our suggestion is that this complex should have the chemical form Xe-H_4. Indeed, looking at Fig. 6(c), it will be noticed that the intense correlation peak at $r \sim 3.5$ Å in $g_{\text{H-H}}(r)$ may contain also contributions from the H-H correlations within the molecular complex and that its position is in agreement with the presence of tetrahedral molecules of the type Xe-H_4. We recall that there is at least another case in which Xe forms molecular complexes, namely, Xe-F_4 [9].

The second result we want to stress is the failure of the LJ potential model in simulating both the H_2-Xe and H_2-H_2 correlations, while it turns out to be a quite good approximation for the Xe-Xe distribution. What is more surprising is that our experimental results indicate that the effective hard-core diameter of the H_2 molecules in this mixture appears to be $\sim 20\%$ higher than the LJ value reported in the literature for pure fluid H_2 [18]. This anomaly is observed in the H_2-H_2 correlations, thus it cannot be ascribed to a failure of the Lorentz-Berthelot combination rule.

As a second step we present our ideas about the features of the microscopic structure of these supercritical mixtures and their relationships with the behavior of the critical line of the demixing transition. Since in all the three supercritical mixtures examined up to now (i.e., He-Xe, Ne-Xe, and H_2-Xe) the Xe-Xe correlations turn out to be the same, and moreover independent of the lighter component, they cannot determine by themselves the type of the demixing transition. It would be interesting to investigate up to what value of the effective hard-core dimension of the second component the Xe network would remain undistorted.

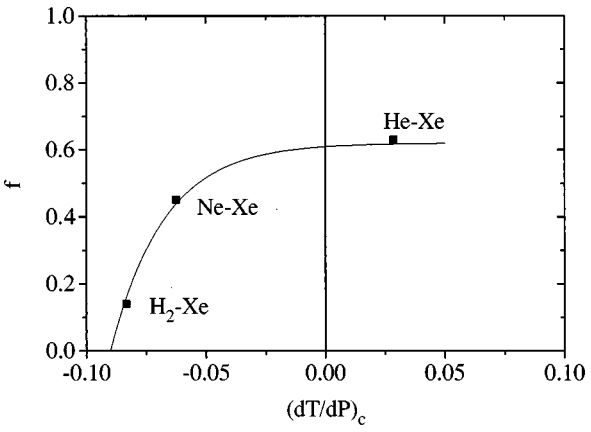

FIG. 9. Fraction f (see the text) as a function of $(dT/dp)_c$ for three mixtures in which the concentration of lighter component is $\sim 20\%$. The points refer to the mixtures that are indicated. The curve is a guide for the eye.

In contrast, among the three mixtures we find different behaviors in the correlation functions that contain the lighter component. In a previous work [6] we already pointed out that these correlations can be related to the type of demixing transition taking place; in particular, we believe that it depends on the value of the fraction f, namely, the fraction of near neighbors of the lighter component within the hard-core distance of the larger component. To show more clearly this connection we report in Fig. 9 the value of f as a function of $(dT/dp)_c$ for the three mixtures. As we can see, the boundary between the first- and second-type behaviors occurs for $f \sim 0.60$. This f value would be found in the He-CH_4 mixture according to the thermodynamic data [1]. Work is now in progress to verify whether or not this is true.

[1] G. M. Schneider, Adv. Chem. Phys. **17**, 1 (1970).
[2] A. J. De Swaan and G. A. M. Diepen, J. Chem. Phys. **44**, 2322 (1966).
[3] J. A. Schouten, Phys. Rep. **172**, 34 (1989).
[4] R. Senesi (unpublished).
[5] M. C. Bellissent-Funel, U. Buontempo, A. Filabozzi, M. Nardone, and F. P. Ricci, Phys. Rev. A **46**, 1002 (1992).
[6] M. Nardone, F. P. Ricci, A. Filabozzi, and P. Postorino, Phys. Rev. E **54**, 6381 (1996).
[7] A. Michels, T. Wassenaar, and P. Louwerse, Physica (Amsterdam) **20**, 99 (1954).
[8] G. A. Cook, *Argon, Helium and the Rare Gases* (Interscience, New York, 1961), Vol. 1.
[9] *CRC Handbook of Chemical and Physical Properties* (CRC, Boca Raton, FL, 1990).
[10] A. K. Soper, in *Advanced Neutron Sources 1988*, edited by D. K. Hyer, IOP Conf. Proc. No. 97 (IOP, Bristol, 1989).
[11] A. K. Soper, W. S. Howells, and A. C. Hannon, Rutheford Appleton Laboratory Report No. RAL-89.046, 1989 (unpublished).
[12] P. A. Egelstaff, in *Methods of Experimental Physics. Neutron Scattering*, edited by K. Skold and D. L. Price (Academic, Orlando, 1986), Vol. 23, Pt. B.
[13] V. F. Sears, Neutron News **3**, 26 (1992).
[14] S. F. Mughabghab, M. Divadeemam, and N. E. Halden, *Neutron Cross Sections* (Academic, New York, 1981), Vol. 1, Pt. A.
[15] U. Buontempo, P. Postorino, M. A. Ricci, and A. K. Soper, Mol. Phys. **81**, 217 (1994).
[16] A. K. Soper, Chem. Phys. **107**, 61 (1986); A. K. Soper, C. Andreani, and M. Nardone, Phys. Rev. E **47**, 2598 (1993).
[17] C. G. Gray and K. E. Gubbins *Theory of Molecular Liquids* (Clarendon, Oxford, 1984), Vol. I.
[18] J. O. Hirschfelder, C. R. Curtis, and R. B. Bird, *Molecular Theory of Gases and Liquids* (Wiley, New York, 1954).
[19] P. A. Egelstaff, D. I. Page, and J. G. Powles, Mol. Phys. **20**, 881 (1971).